Journal of Applied Pharmaceutical Research
Volume 14 Issue 2, Year of Publication 2026, Page 220 – 238
DOI: https://doi.org/10.69857/joapr.v14i2.1182

Check for updates

Research Article

JOURNAL OF APPLIED PHARMACEUTICAL RESEARCH | JOAPR
www.japtronline.com ***ISSN: 2348 – 0335***

COMPUTATIONAL INSIGHTS INTO TAXIFOLIN'S THERAPEUTIC MECHANISMS FOR ALZHEIMER'S DISEASE

Ashif Anjukandan*, Rajaganapathy Kaliyaperumal

Article Information
Received: 12th October 2025
Revised: 10th January 2026
Accepted: 15th February 2026
Published: 15th March 2026

Keywords
Taxifolin, Alzheimer's, Lipinski's, Network pharmacology, molecular simulation.

ABSTRACT
Background: Alzheimer's disease (AD) poses a significant challenge for research. Taxifolin is a natural flavonoid and has potential in protecting against Alzheimer's by inhibiting oxidative stress. This study aims to elucidate the multi-target effects of Taxifolin on Alzheimer's disease by computational techniques. **Materials and Methods:** The target genes were mapped into a PPI network using the STRING database. Hub genes were identified using Cytoscape software. Gene Ontology and KEGG pathway analyses were performed to identify AD-related pathways. Finally, docking analysis was performed using CDOCKER and Autodock, and GROMACS molecular dynamics simulations were performed to study the ligand's behaviour. **Results and Discussion:** The results revealed promising drug-like properties, as assessed by Lipinski's rule and ADMET predictions. A total of 47 human genes showed significant similarity (≥ 0.70), with 10,234 targets linked to Alzheimer's disease. Of these, 673 genes were highly associated with the disease (GDA > 0.1). A Venn diagram identified 16 overlapping genes, including BACE1, DPP4, PIK3CA, MTOR, ESR2, and APP. Network analysis revealed interactions among Taxifolin, MTOR, SERPINE1, ESR2, PIK3CA, and NOS3. Taxifolin docking against Alzheimer's targets identified 5T4B as the best hit, with the lowest binding energy in CDOCKER (−43.57 kcal/mol) and AutoDock Vina (−8.8 kcal/mol). A 100-ns MD simulation confirmed a stable 5T4B–taxifolin complex, showing structural stability (RMSD/RMSF), compactness (Rg), solvent exposure (SASA), and persistent hydrogen bonds. MM-PBSA analysis supported strong binding, primarily driven by van der Waals and electrostatic interactions. **Conclusion:** Hence, the study offers insights into the multi-target mechanisms of Taxifolin against AD.

INTRODUCTION

According to Alzheimer's disease (AD) facts and figures 2024, it is the most common cause of dementia, resulting in 60% - 80% of cases. Beta-amyloid protein and tau protein play a major part in causing the disease. Twisted strands of tau-protein inside the neuron and the accumulation of beta-amyloid protein outside the neuron result in neuron death and damage to brain tissue [1]. There was 146.2% increase in AD-related death from 2000 to 2018 [2]. Being multifactorial, the risk factors for AD include: genetic susceptibility (APOE gene); vascular pathway;

**Department of Pharmacology, Faculty of Pharmacy, Bharath Institute of Higher Education and Research, Chennai, Tamil Nadu, India.*

For Correspondence: **ashifak.research@gmail.com**

nutritional and dietary factors, such as vitamin B12 and antioxidant deficiencies; traumatic head injuries and exposure to toxins, etc. [3]. Early-onset AD results from autosomal dominant mutations in the amyloid precursor protein, presenilin-1, and presenilin-2 genes [4]. According to a study, the APOE ε4 allele is a causative genetic factor for both early- and late-onset AD [5]. Exposure to non-steroidal anti-inflammatory drugs (NSAIDS) results in 19% reduction in AD risk [6]. A meta-analysis reported that low-dose aspirin did not affect cognitive function. Thus questioning the role of NSAIDS in AD treatment [5]. The FDA has approved two drug categories for treating AD: cholinesterase inhibitors for early-stage disease, which target acetylcholine degradation, and N-methyl-d-aspartate (NMDA) receptor blockers, along with AChE inhibitors, for managing further disease progression [7]. Medicinal plants have proved effective in controlling SARS-CoV-2, cancers, inflammation, cardiovascular disorders, and neurodegenerative disorders [9]. Extracts from Voacanga Africana and Eriodictyon californicum, and the flavanol fisetin, showed significant ability to prevent oxytosis/ferroptosis [8]. Phenotypic screening assays, including Oxytosis/ferroptosis, in vitro ischemia, Microglial activation, Trophic factor withdrawal, PC12 neurites, and Intracellular Aβ toxicity of plant-based compounds, paved the way for using plants as a source of prospective treatment for AD. Flavonoids found in foods such as onions and olive oil have positive pharmacological activities & favourable therapeutic effect [10]. The incorporation of computer-aided drug design (CADD) into modern drug design is driven by recent advances in computational power and technology [11]. The computational (in-silico) techniques include database mining, quantitative structure-activity relationships, pharmacophores, homology modeling, and other molecular modeling approaches. Recent computational approaches, such as machine learning, data mining, network analysis, and data analysis tools, were also incorporated [12]. The majority of these techniques are used in conjunction with in vitro data to develop models that facilitate the identification of novel molecules [13]. Thus, we conducted an in-silico analysis to assess the preventive properties of taxifolin in AD.

MATERIALS AND METHODS

Pharmacokinetic properties and toxicity prediction

The PubChem database (https://pubchem.ncbi.nlm.nih.gov) was used to retrieve the canonical SMILES for taxifolin. SwissADME (http://www.swissadme.ch) was used to analyze the drug-likeness and physicochemical properties of taxifolin, including its ADME properties. Finally, the toxicity of taxifolin was assessed using OSIRIS, a tool available at https://www.cheminfo.org/flavor/cheminformatics/Utility/Propertyexplorer/index.htm

Taxifolin-Target Prediction

A free online Binding DB database covers protein interactions with small drug-like compounds. It was connected to numerous databases, and these connections were used to extract further information regarding the targets. Using SMILES and the "homo sapiens" setting in Binding DB https://www.bindingdb.org/bind/index.jsp, with the "minimum needed interaction score" set to "high confidence (0.7)" throughout the prediction phase, the target genes were evaluated in Binding DB.

Disease-Target Prediction

The potential targets were selected from http://www.disgenet.org using the term “Alzheimer’s disease”. The target's standard name was obtained from UniProtKB, specifying the organism as "Homo sapiens.” The DisGeNET database was utilized to determine the gene-disease association (GDA) score, which was used to rank the association between genes and AD. In this study, targets with a GDA score greater than 0.1 were considered to be highly correlated with AD. A GDA threshold of >0.1 was used to balance sensitivity and specificity, thereby including genes with relevant disease associations while minimizing the inclusion of weakly supported links. Although more stringent cutoffs (e.g., >0.2 or >0.3) effectively reduce false-positive rates, they may inadvertently exclude emerging or less-characterized genes that could be biologically significant but have not yet been extensively validated.

Intersection of related targets

To more accurately assess the overlap between AD-related targets and taxifolin targets, we merged the two sets and created Venn diagrams using an online tool at http://bioinformatics.psb.ugent.be/webtools/Venn.

The overlapping targets were selected for further analysis as potential therapeutic targets.

Construction and analysis of Protein-Protein Interaction (PPI) network

The overlapping targets were then imported into the STRING database (version 11.0) to construct a PPI network: https://stringdb.org/. The criteria for selecting the human

organism were a minimum interaction score of greater than 0.4. Only interactions that met this criterion were deemed significant. PPI networks are composed of nodes representing target proteins and edges representing protein interactions. The thickness of an edge is proportional to the combined score of the interaction. The degree of a node refers to the number of other nodes directly connected to it. A higher degree indicated a node of greater importance. Following its development, this network was subsequently imported into Cytoscape (Version 3.10.1) to visualize and analyze its structure. The Cytoscape software may be obtained from the Cytoscape website: https://cytoscape.org/. The degree was calculated to identify core targets using CytoHubba. This gives the count of direct neighbours. In this study, the top 10 proteins ranked by degree were selected as core targets.

GO and Kyoto Encyclopedia of genes and genomes (KEGG) enrichment analysis

DisGeNET keyword: The analysis of gene ontology and KEGG enrichment pathways was conducted using the Database for Annotation, Visualization, and Integrated Discovery (DAVID), available at https://david.ncifcrf.gov/. The DAVID functional annotation tool was utilized to allocate functional roles at three levels - cellular component (CC), molecular function (MF), and biological process (BP) - to a selection of critical genes. DAVID is a functional enrichment database accessible through the Web, enabling researchers to comprehend the bioactivity of a multitude of genes. In the current study, a significance level of ≤0.05 was set, and the top 10 GO enrichments and top 10 KEGG pathways were selected for further analysis. These results were then visualized using an online tool available at http://www.bioinformatics.com.cn.

Molecular Docking

The target proteins of Alzheimer's Disease were obtained from the Protein Data Bank. Docking protocol validation involved re-docking the native co-crystallized ligand into each target protein's binding site using the CDOCKER module in BIOVIA Discovery Studio (version X.X). The co-crystallized ligands were extracted from the PDB structures, and the protein was prepared by removing crystallographic water molecules, adding hydrogens, applying the CHARMm force field, and defining the binding site based on the XYZ coordinates of the ligand. Using the default setup, 2000 dynamics steps (at a 0.002 ps time step), heating to 700 K over 2000 steps, and cooling to 300 K over 5000 steps were performed. For each protein–ligand system, ten random ligand orientations were generated and clustered with an RMSD cutoff < 2 Å, and the best pose was ranked by the CDOCKER interaction energy score. After validation, the ligand taxifolin was docked into each target protein's binding pocket. Ten poses were generated per complex, clustered at an RMSD < 2 Å, and the best were selected based on the CDOCKER score. To confirm docking reliability, comparative docking with Auto Dock Vina (v1.2.1) was performed for both the co-crystallized ligand and taxifolin using the same binding-site definition. The binding affinities & orientations from Vina were then compared with the CDOCKER results. For computational efficiency, MM-PBSA calculations were performed only on the top-ranked taxifolin–protein complex (selected based on CDOCKER/Vina results) to refine the binding free-energy estimate.

Molecular Dynamics

MD simulations were performed in triplicate by varying the velocities of the production run using Gromacs version 2024.4. The 5T4B-Taxifolin complex, which exhibits the lowest binding energy (indicating the strongest affinity), was analyzed using molecular dynamics simulations. MD simulations were carried out for 100 ns using GROMACS version 2024.4. The conformational stability of the complex was examined in a solvated water model containing ordered water molecules. The CHARMM force field was employed. The system was solvated with explicit TIP3P water molecules in a cubic box measuring $9.0 \times 9.0 \times 9.0$ nm³, with a 2 nm distance between the box edges and the protein. The MD system included 766 amino acids, totaling 82449 atoms after solvation. Necessary counterions (0.15 M NaCl) were added to neutralize the net charge of the system. Energy minimization was performed using the steepest descent algorithm. A 50ps position-restrained simulation was conducted to allow the solvent to equilibrate around the protein. Continuous pressure of 1 bar and temp. of 300 K were maintained using Berendsen's coupling algorithm, with an integration timestep of 2 femtoseconds. Trajectories were saved every 10 ps, resulting in 10,000 frames. The generated trajectories were analyzed for RMSD, RMSF, radius of gyration (Rg), SASA, and hydrogen-bonding interactions between the protein and the ligand. Results were analyzed using GROMACS's built-in tools. RMSD and RMSF calculations were performed on backbone atoms. Graphs were plotted using xmgrace. The protein conformation and its interactions with small molecules at different time scales (ns) were visualized with VMD & Discovery Studio Visualizer v21.

Table 1: The physicochemical properties of Taxifolin

Compound	Molecular Wt.	Clog P	tPSA	HBD	HBA
Successful CNS drugs	<400	<5	<90	<3	<7
Taxifolin	304.25	0.96	127.45	5	7

Table 2: The ADMEtox properties of Taxifolin

Ligand	Mutagenicity	Tumorigenicity	Skin Irritation	Reproductive effective
Taxifolin	safe	safe	Safe	safe

Table 3: The pharmacokinetic properties of Taxifolin

Category	Property	Value
Structure	SMILES	Oc1cc2Oc(c3ccc(c(3)O)O)OC(C(=O)c2c(1)O)O
	Formula	C15H12O7
Physicochemical Properties	Molecular weight	304.25 g/mol
	Num. heavy atoms	22
	Num. arom. heavy atoms	12
	Fraction Csp3	0.13
	Num. rotatable bonds	1
	Num. H-bond acceptors	7
	Num. H-bond donors	5
	Molar Refractivity	74.76
	TPSA	127.45 Å²
Lipophilicity	Log Po/w (iLOGP)	1.3
	Log Po/w (XLOGP3)	0.95
	Log Po/w (WLOGP)	0.86
	Log Po/w (MLOGP)	-0.64
	Log Po/w (SILICOS-IT)	0.66
	Consensus Log Po/w	0.63
Water Solubility	Log S (ESOL)	-2.86
	Solubility (ESOL)	6.62e-01 mg/ml; 2.18e-03 mol/l
	Class (ESOL)	Soluble
Pharmacokinetics	GI absorption	High
	BBB permeant	No
	P-gp substrate	No
	CYP1A2 inhibitor	No
	CYP2C19 inhibitor	No
	CYP2C9 inhibitor	No
	CYP2D6 inhibitor	No
	CYP3A4 inhibitor	No
	Log Kp (skin permeation)	-7.48 cm/s
Druglikeness	Lipinski	Yes; 0 violation
	Ghose	Yes
	Veber	Yes
	Egan	Yes
	Muegge	Yes
	Bioavailability Score	0.55
Medicinal Chemistry	PAINS	1 alert: catechol_A
	Brenk	1 alert: catechol
	Leadlikeness	Yes
	Synthetic accessibility	3.51

MMPBS Analysis

The stable trajectories from the MD simulation for 50ns were subjected to MMPBSA analysis using gmx ana V 1.5. The total binding free energy (ΔG bind) of a ligand–protein complex is determined by the following equation,

$$\Delta Gbind = G\,complex - (G\,protein + G\,ligand)$$

Where G can be computed using Poisson–Boltzmann (PB) models for solvation.

The total decomposition energy contributed by each residue due to interaction with the ligand was estimated using parameters such as Electrostatic, van der Waals, polar, nonpolar, solvation energy, and GGas.

RESULT AND DISCUSSION

Pharmacokinetics properties and toxicity prediction

Pharmacophoric analysis of taxifolin showed that the drug fell under the criteria of successful CNS drug molecules whose molecular weight should be less than 400g/mol, ClogP should be less than 5, topological polar surface area should be ~90Å², number of hydrogen bonding donors should be less than 3, and number of hydrogen bonding acceptors should be less than 7. The molecule is less lipophilic and more soluble.

Table 4: Targets of taxifolin

Sl.No	Gene	UniProt ID	Decription
1	CBR4	Q8N4T8	3-oxoacyl-[acyl-carrier-protein] reductase
2	PGD	P52209	6-phosphogluconate dehydrogenase, decarboxylating
3	ADAMTS4	O75173	A disintegrin and metalloproteinase with thrombospondin motifs 4
4	ADAMTS5	Q9UNA0	A disintegrin and metalloproteinase with thrombospondin motifs 5
5	ACHE	P22303	Acetylcholinesterase
6	ALPL	P05186	Alkaline phosphatase, tissue-nonspecific isozyme
7	FUT7	Q11130	Alpha-(1,3)-fucosyltransferase 7
8	SNCA	P37840	Alpha-synuclein
9	APP	P05067	Amyloid-beta precursor protein
10	Bcl-2	P10415	Apoptosis regulator Bcl-2
11	ARG1	P05089	Arginase 1
12	CYP19A1	P11511	Aromatase
13	ABCB1	P08183	ATP-dependent translocase ABCB1
14	BACE1	P56817	Beta-secretase 1
15	CA1	P00915	Carbonic anhydrase 1
16	CA12	O43570	Carbonic anhydrase 12
17	CA2	P00918	Carbonic anhydrase 2
18	CA4	P22748	Carbonic anhydrase 4
19	CA7	P43166	Carbonic anhydrase 7
20	CSNK1E	P49674	Casein kinase I isoform epsilon
21	CYP4A11	Q02928	Cytochrome P450 1B1
22	DPP4	P27487	Dipeptidyl peptidase 4
23	DNMT1	P26358	DNA (cytosine-5)-methyltransferase 1
24	RAD52	P43351	DNA repair protein RAD52 homolog
25	CLK1	P49759	Dual specificity protein kinase CLK1
26	CLK4	Q9HAZ1	Dual specificity protein kinase CLK4
27	DYRK1A	Q13627	Dual specificity tyrosine-phosphorylation-regulated kinase 1A
28	DYRK1B	Q9Y463	Dual specificity tyrosine-phosphorylation-regulated kinase 1B
29	MECR	Q9BV79	Enoyl-[acyl-carrier-protein] reductase, mitochondrial
30	ESR2	Q92731	Estrogen receptor beta
31	G6PD	P11413	Glucose-6-phosphate 1-dehydrogenase
32	HSP90AB1	P08238	Heat shock protein HSP 90-beta
33	MAPKAPK5	Q8IW41	MAP kinase-activated protein kinase 5
34	NADK	O95544	NAD kinase
35	NOS3	P29474	Nitric oxide synthase, endothelial
36	PIK3CA	P42336	Phosphatidylinositol 4,5-bisphosphate 3-kinase catalytic subunit alpha isoform
37	PGAM1	P18669	Phosphoglycerate mutase 1
38	SERPINE1	P05121	Plasminogen activator inhibitor 1
39	PDGFRA	P16234	Platelet-derived growth factor receptor alpha
40	ALOX5	909917	Polyunsaturated fatty acid 5-lipoxygenase
41	PSMB5	P28074	Proteasome subunit beta type-5
42	MTOR	P42345	Serine/threonine-protein kinase mTOR
43	SHBG	P04278	Sex hormone-binding globulin
44	STAT1	P42224	Signal transducer and activator of transcription 1-alpha/beta
45	SQLE	Q14534	Squalene monooxygenase
46	TERT	O14746	Telomerase reverse transcriptase
47	TTR	P02766	Transthyretin

The pharmacokinetic properties show that the molecule is highly absorbable in the gastrointestinal tract. It is a non-BBB-permeant, non-CYP inhibitor and doesn't form a P-gp substrate. Thus, it is non-hepatotoxic. The molecule is found to exhibit drug-like properties. It was observed that the molecule is non-mutagenic and non-tumorigenic. It doesn't cause any skin irritation and is also effective. The physicochemical properties, pharmacokinetic, and ADMETox properties of Taxifolin are shown in Table 1, Table 2 & Table 3.

Taxifolin-Target Prediction

When predicting the targets of taxifolin, 47 genes in Homo sapiens showed similarity >/= 0.70. The targets of taxifolin obtained from BindingDb have been included in Table 4.

Disease-Target Prediction

There were around 10234 targets directly or indirectly associated with the disease. Among these, 673 genes were highly associated with the disease, with GDA > 0.1. The list of targets is included in Supplementary Table 1 (uploaded on website as separate file).

Intersection of related targets

While finding the common genes among these target groups (drug targets and disease targets) a Venn diagram have been plotted and found that 16 genes namely ALOX5, TTR, BACE1, DPP4, PIK3CA, NOS3, ABCB1, MTOR, SERPINE1, CYP19A1, DYRK1A, ADAMTS4, SNCA, ESR2, ACHE, and APP were found to be overlapping among disease targets and taxifolin targets. The Venn diagram of the overlapping targets between taxifolin and the disease is shown in Figure 1.

Construction and analysis of the PPI network

Centrality metrics in protein–protein interaction (PPI) networks are highly relevant to complex diseases such as Alzheimer's disease (AD), as they facilitate the identification of topologically essential proteins whose perturbation can lead to systemic network instability. These hub proteins often integrate signals across multiple pathological pathways, positioning them as critical nodes for elucidating disease pathogenesis and prioritizing targets for therapeutic intervention.

Figure 2 displays the integrated network combining protein–protein interactions (PPI), protein–drug interactions (PDI), disease–drug, and disease–target relationships based on overlapping genes. Network analysis revealed that the genes were interconnected and interacted with taxifolin.

Notably, BACE1, DPP4, PIK3CA, MTOR, ESR2, and APP showed strong links to Alzheimer's disease. Additionally, taxifolin was observed to interact with MTOR, SERPINE1, ESR2, PIK3CA, and NOS3 within this network.

Although the network provides insights into potential molecular interactions, it is essential to note that many protein–protein interactions are transient or exhibit low binding affinities, which can limit their detectability with conventional experimental approaches.

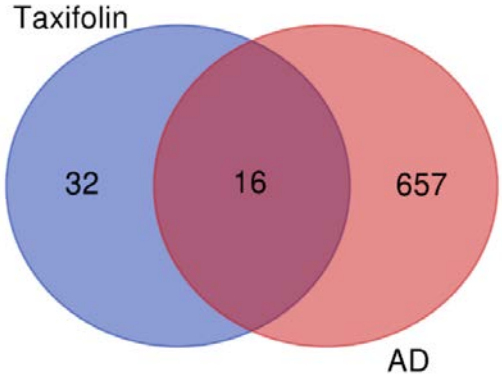

Figure 1: The Venn diagram of overlapping genes

Additionally, protein–protein interactions are often context-dependent and may occur only under specific biological conditions, such as particular cell types, developmental stages, or environmental stimuli.

Consequently, interactions observed in one biological context may not be universally applicable. KEGG pathway and Gene Ontology analyses based on raw p-values suggested associations of the overlapping targets with pathways related to Alzheimer's disease, endocrine resistance, AGE–RAGE signaling & insulin resistance. However, the Benjamini–Hochberg false discovery rate–adjusted values for all pathways exceeded 0.05. So, the identified pathway associations are presented for exploratory interpretation and provide biological context rather than definitive enrichment.

GO and Kyoto Encyclopedia of genes and genomes (KEGG) enrichment analysis

The gene ontology terms and their corresponding subgroups, based on gene counts and p-values, are represented graphically in Figures 3 and 4 and in Table 5. Moreover, these genes were found to be involved in pathways: AGE-RAGE signalling pathway in diabetic complications, Chemical carcinogenesis - receptor activation, Endocrine resistance, and HIF-1 signalling pathway.

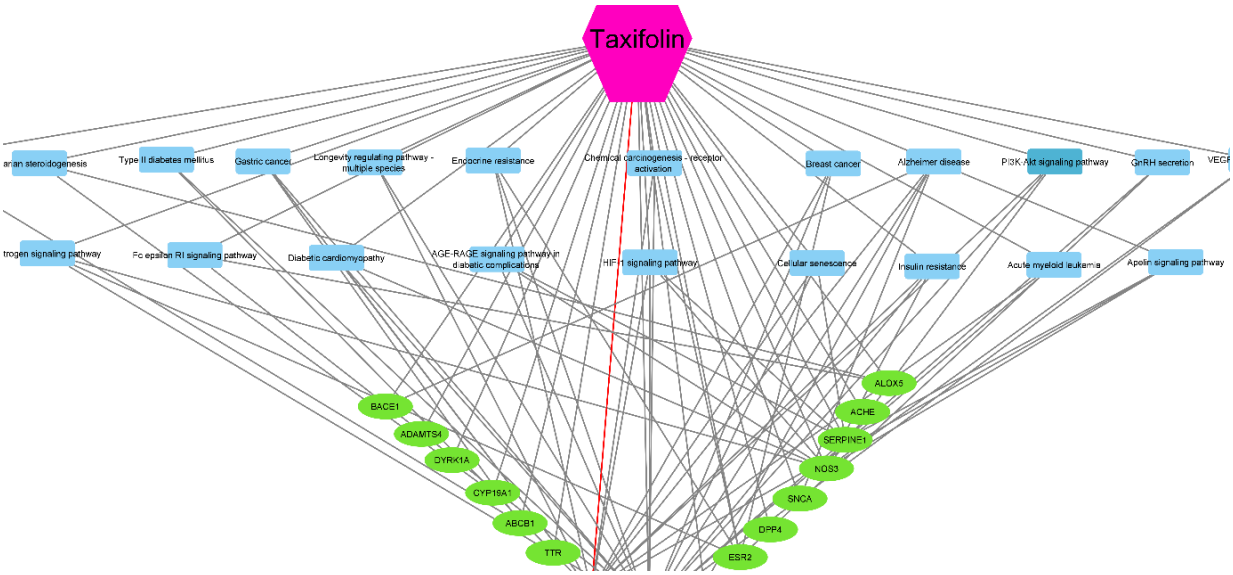

Figure 2: The merged network

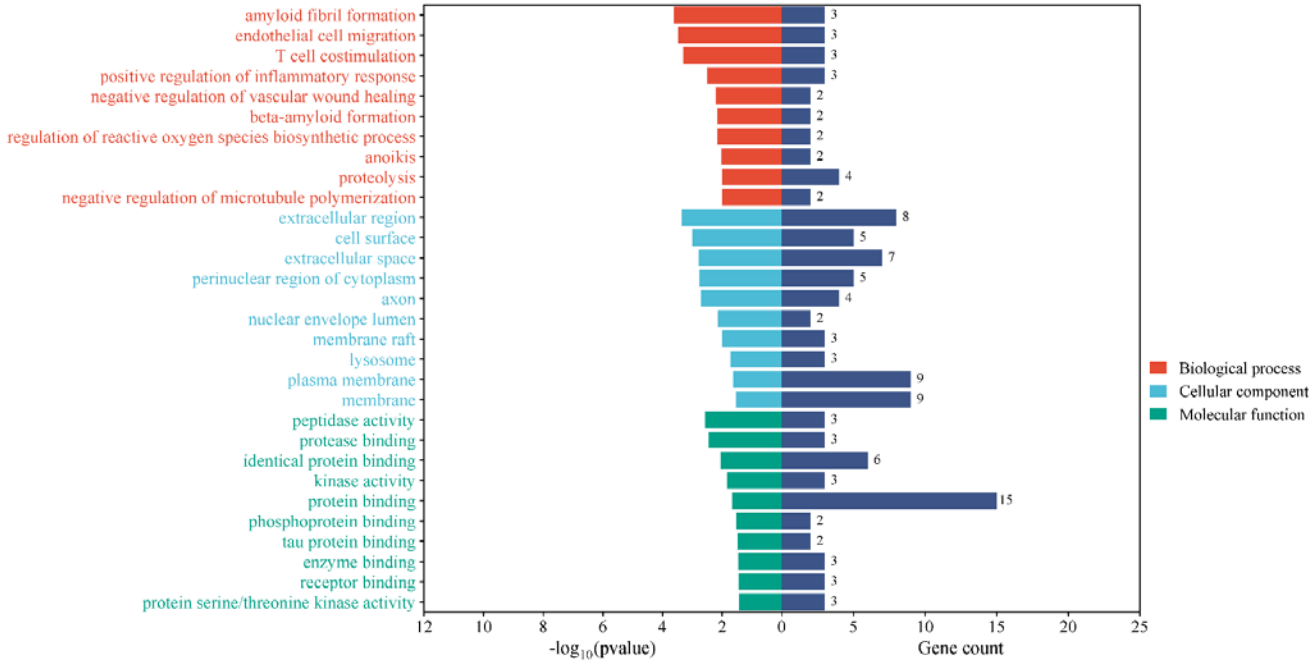

Figure 3: GO and KEGG pathway association analysis.

Table 5: KEGG Pathway Associations based on raw p-values

Pathways	Enrichment	p-value	Count
Alzheimer disease	8.056175595	0.001976	5
Chemical carcinogenesis - receptor activation	8.755390836	0.038945	3
Endocrine resistance	18.94023324	0.009112	3
AGE-RAGE signaling pathway in diabetic complications	18.56142857	0.009474	3
Insulin resistance	17.18650794	0.010984	3
Estrogen signaling pathway	13.54848801	0.017281	3
Apelin signaling pathway	13.35354573	0.017761	3
Breast cancer	12.62682216	0.019738	3
Gastric cancer	12.45733461	0.020247	3
Cellular senescence	11.89835165	0.02207	3

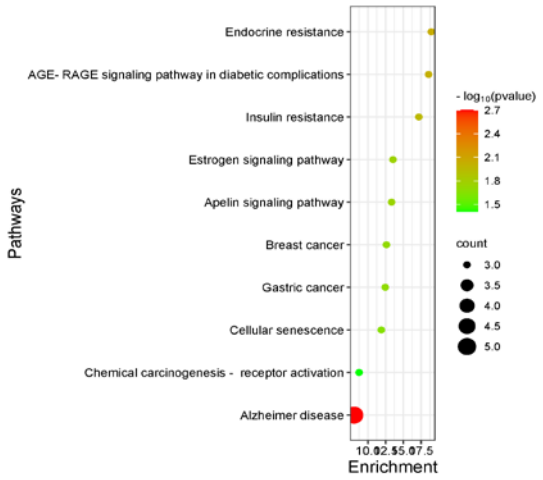

Figure 4: The KEGG pathway bubble plot based on raw p-values and gene counts. The p >0.05 after Benjamini-Hochberg FDR correction.

Molecular Docking studies

To validate the docking protocol, different target proteins of Alzheimer's disease were redocked with the co-crystallized ligands using CDOCKER. The CDOCKER interaction energy of the co-crystallized ligands was determined. The redocked poses showed good overlap with the crystallographic conformation, which was determined by RMSD values, and the binding affinities are shown in Table 6. After docking validation, taxifolin was docked into the co-crystallised ligand position; its three-dimensional docked poses and two-dimensional interaction diagrams are reported in Figures 5–13. To further validate docking, comparative scores were predicted by docking the co-crystallized ligands and taxifolin with different target proteins of Alzheimer's disease using AutoDock Vina, and their redocking RMSD and binding affinities are shown in Table 6.

Table 6: Docking and its validation using CDOCKER and AutoDock Vina. Docking scores of co-crystallized ligands and taxifolin against the respective receptors mentioned by their PDB IDs.

PDB-ID chain & resolution	CDOCKER Interaction score (Kcal/mol) Co-crystalized ligand complex (Redocking)	CDOCKER Interaction score (Kcal/mol) Taxifolin complex	Autodock Vina Interaction score (Kcal/mol) for Co-crystalized ligand complex with RMSD (Redocking)	Autodock Vina Interaction score (Kcal/mol) for Taxifolin complex with RMSD
4DRI-A 1.45Å	-41.23 RMSD 1.0 Å	-28.09	-10.3 RMSD 1.2Å	-7.2
2GAB-A 1.85Å	-45.32 RMSD 1.3 Å	-24.99	-5.0 RMSD 1.1Å	-4.6
5HDZ-A 1.49Å	-44.26 RMSD 1.2 Å	-39.99	-9.5 RMSD 1.4Å	-7.9
5T4B-A 1.76Å	-47.83 RMSD 1.0 Å	-43.57	-10.5 RMSD 1.6Å	-8.8
8EXL- A 1.98Å	-48.26 RMSD 1.5 Å	-43.13	-10.8 RMSD 1.9Å	-8.8
6AV7 -A 1.92Å	-43.37 RMSD 1.8 Å	-33.24	-6.7 RMSD 1.2Å	-5.8
8JJV -A 1.23Å	-31.61 RMSD 1.3 Å	-16.31	-6.2 RMSD 3.8Å	-5.6
3OLL -A 1.5Å	-42.58 RMSD 1.0 Å	-43.39	-10.7 RMSD 1.3Å	-7.4
3PMR-A 2.11Å	-39.48 RMSD 1.3 Å	-26.89	-7.5 RMSD 1.8Å	-5.8
4EY7-A 2.3Å	-47.81 RMSD 1.0 Å	Dock Failed	-12.2 RMSD 1.8Å	-1.2

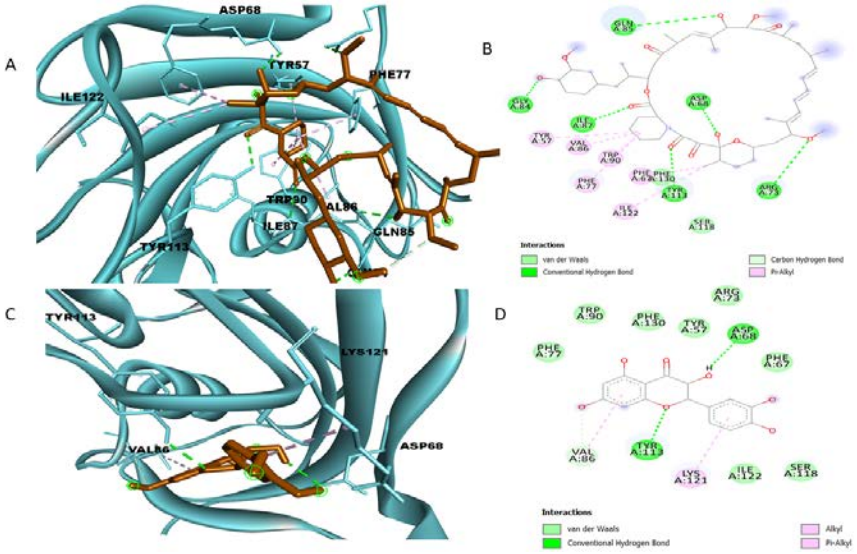

Figure 5: Docking of 4DRI with crystallized ligand's (Rapamycin) 3D and 2D view (A) and (B). Taxifolin 2D and 3D docked poses (C) and (D).

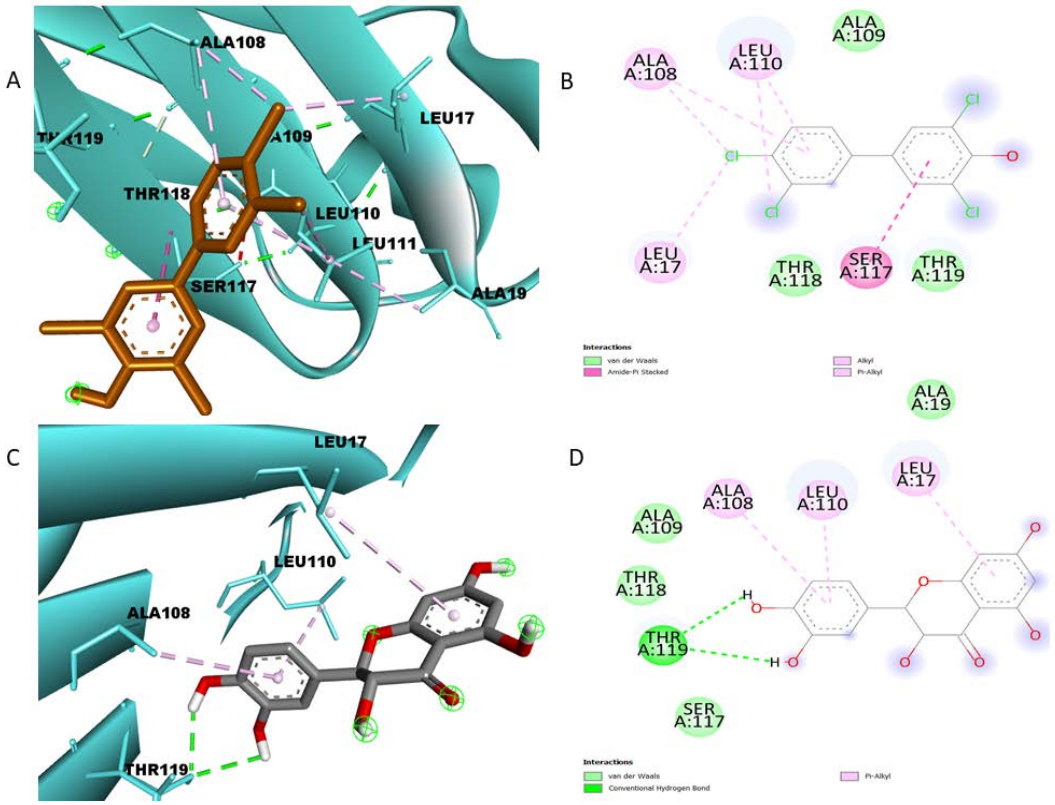

Figure 6: Docking of 2GAB with crystallized ligands (Hydroxylated polychlorinated Biphenyl-4-hydroxy-3,3',5,4'-tetrachlorobiphenyl) 3D and 2D view (A) and (B). Taxifolin 2D and 3D docked poses (C) and (D).

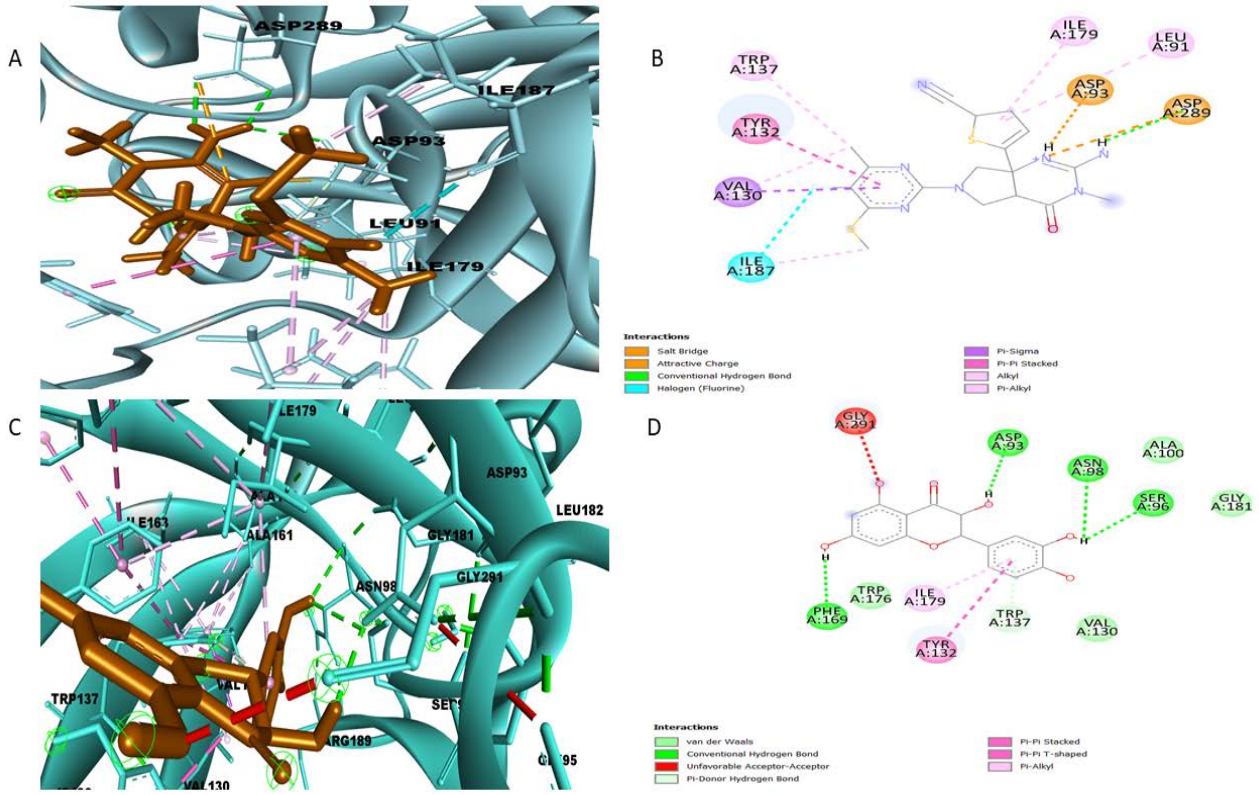

Figure 7: Docking of 5HDZ with crystallized ligands ((7aR)-7a-(5-cyanothiophen-2-yl)-6-(5-fluoro-4-methyl-6-(methylthio) pyrimidin-2-yl)-3-methyl-4-oxooctahydro-2H-pyrrolo[3,4-d]pyrimidin-2-iminium) 3D and 2D view (A) and (B). Taxifolin 2D and 3D docked poses (C) and (D).

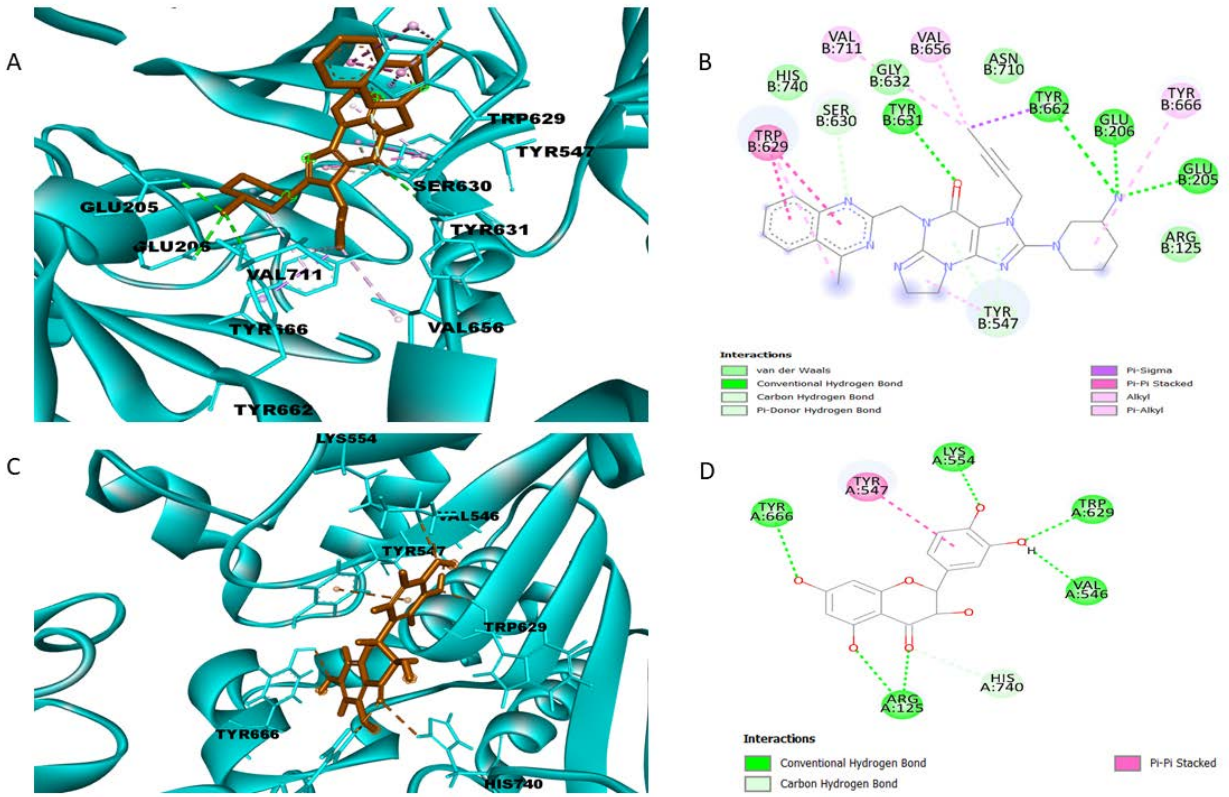

Figure 8: Docking of 5T4B with co-crystallized ligand's (2-[(3R)-3-aminopiperidin-1-yl]-3-(but-2-yn-1-yl)-5-[(4-methylquinazolin-2-yl)methyl]-3H-imidazo[2,1-b]purin-4(5H)-one) 3D and 2D view (A) and (B). Taxifolin 2D and 3D docked poses (C) and (D).

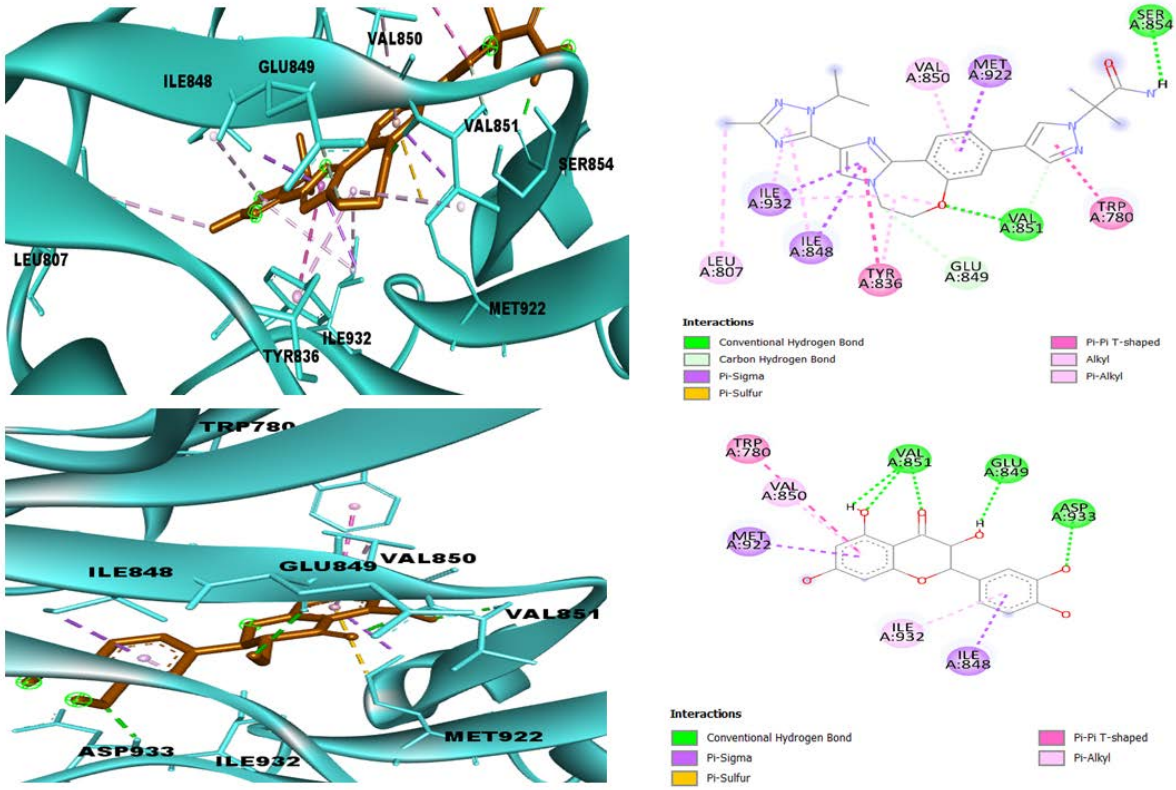

Figure 9: Docking of 8EXL with co-crystallized ligand (Taselisib) 3D and 2D view (A) and (B). Taxifolin 2D and 3D docked poses (C) and (D).

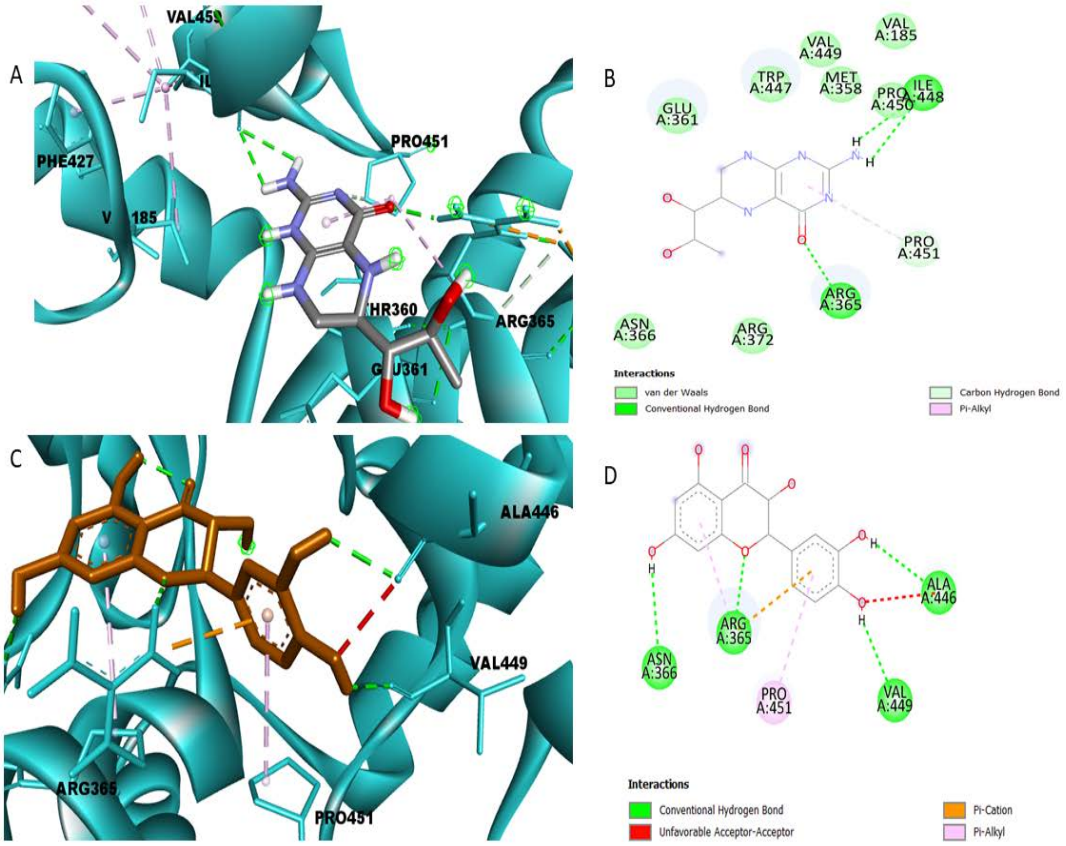

Figure 10: Docking of 6AV7 with co-crystallized ligands (5,6,7,8-Tetrahydrobiopterin), 3D and 2D view (A) and (B). Taxifolin 2D and 3D docked poses (C) and (D).

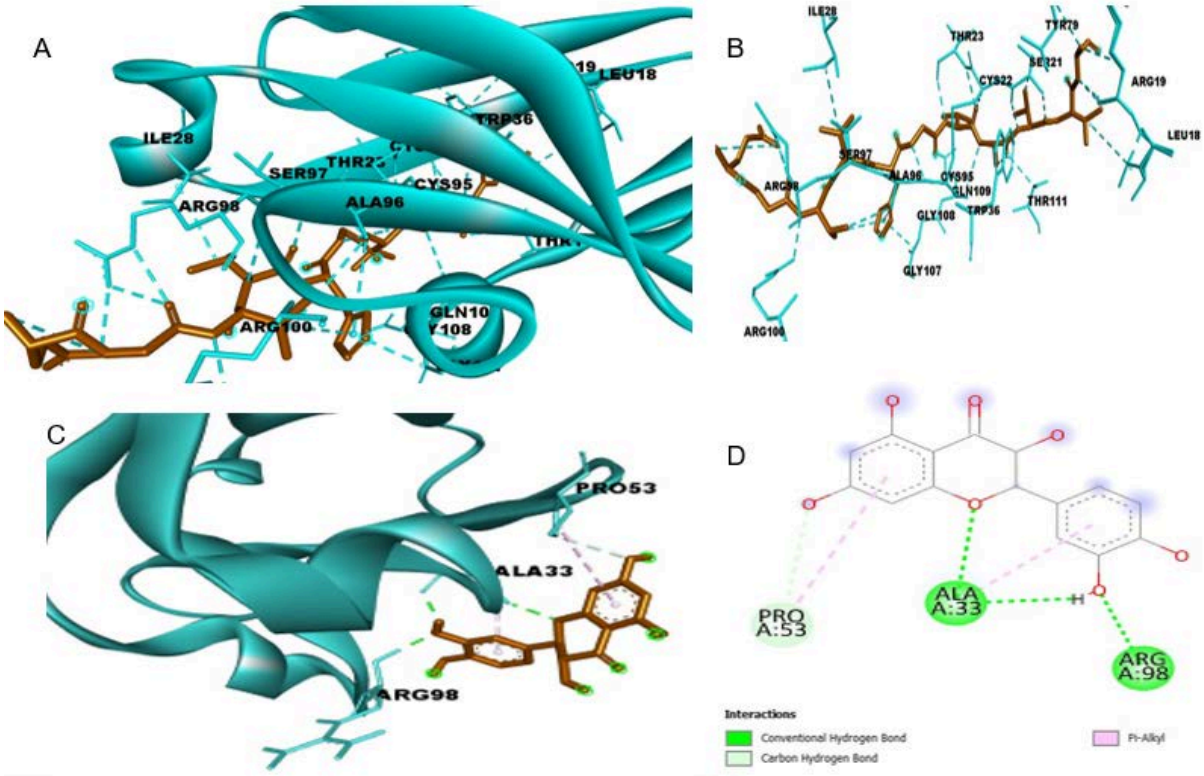

Figure 11: Docking of 8JJV with crystallized ligands (Alpha-synuclein peptide) 3D and 2D view (A) and (B). Taxifolin 2D and 3D docked poses (C) and (D).

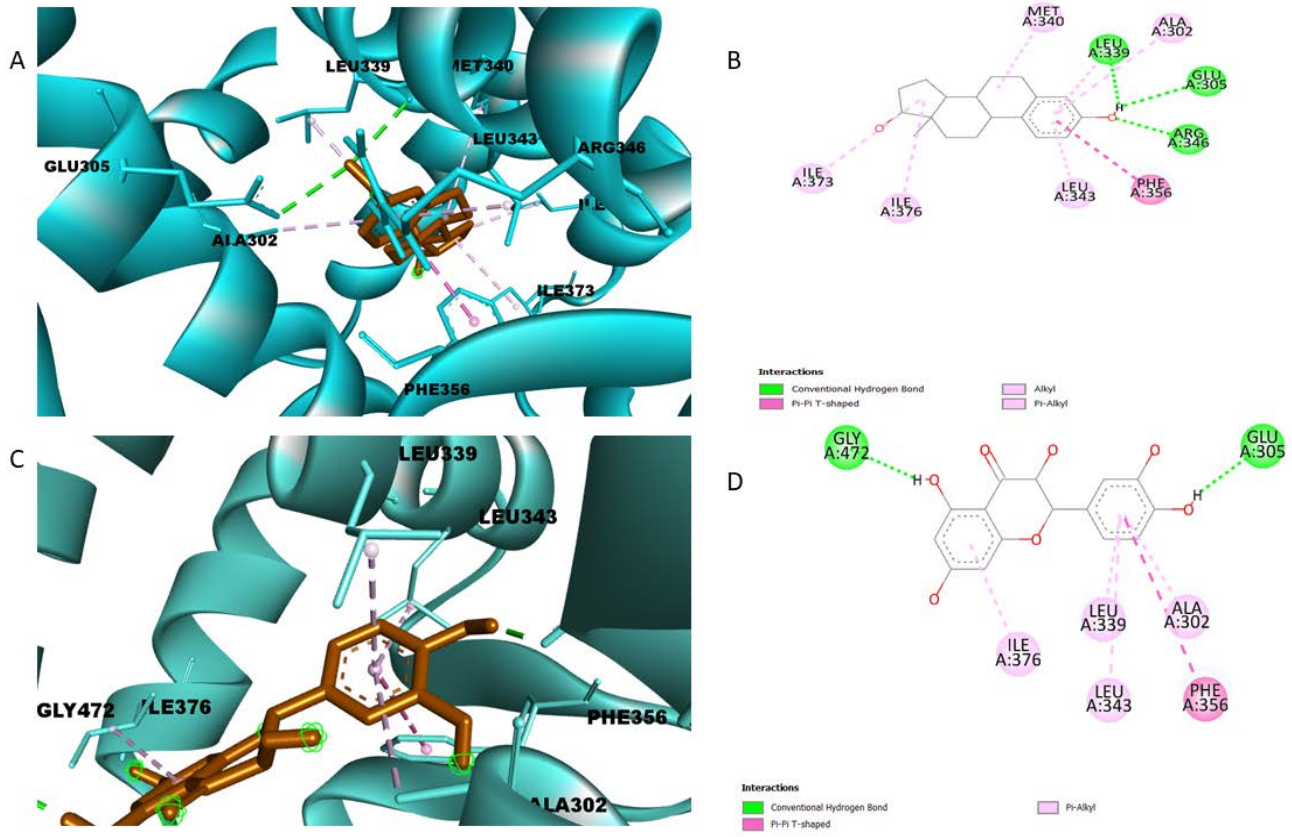

Figure 12: Docking of 30LL with crystallized ligands (Estradiol), 3D and 2D view (A) and (B). Taxifolin 2D and 3D docked poses (C) and (D).

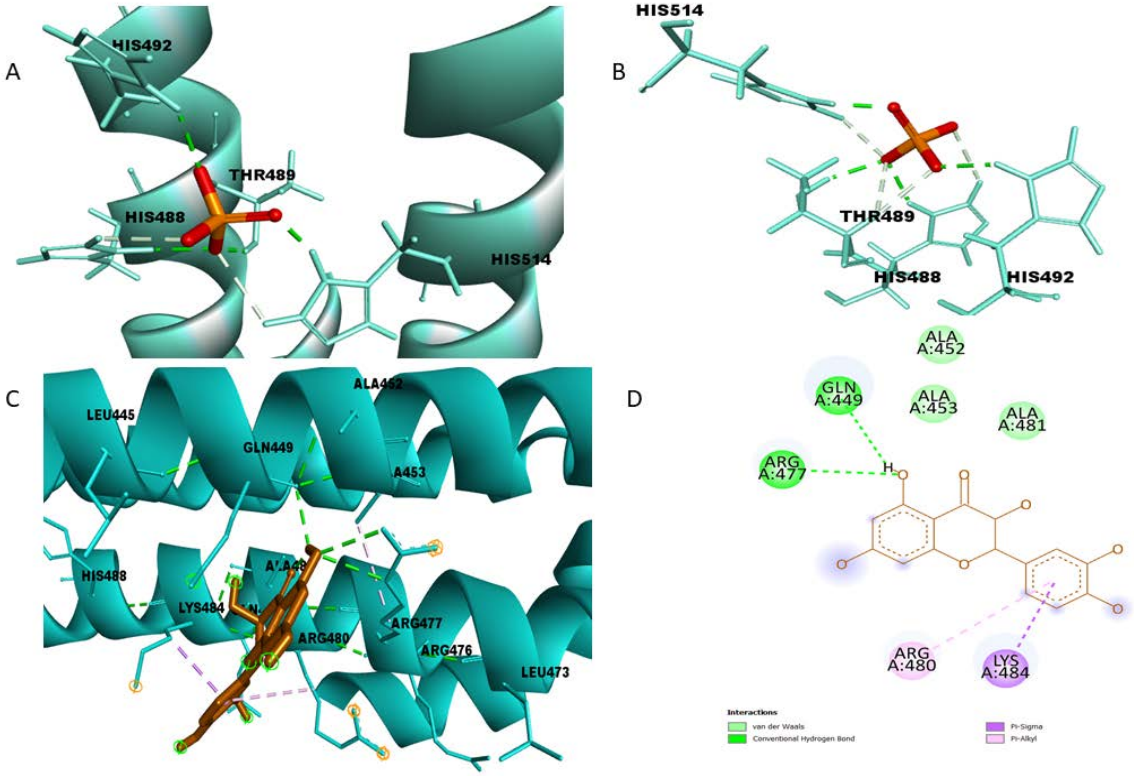

Figure 13: Docking of 3PMR with crystallized ligands (Phosphate ion), 3D and 2D view (A) and (B). Taxifolin 2D and 3D docked poses (C) and (D).

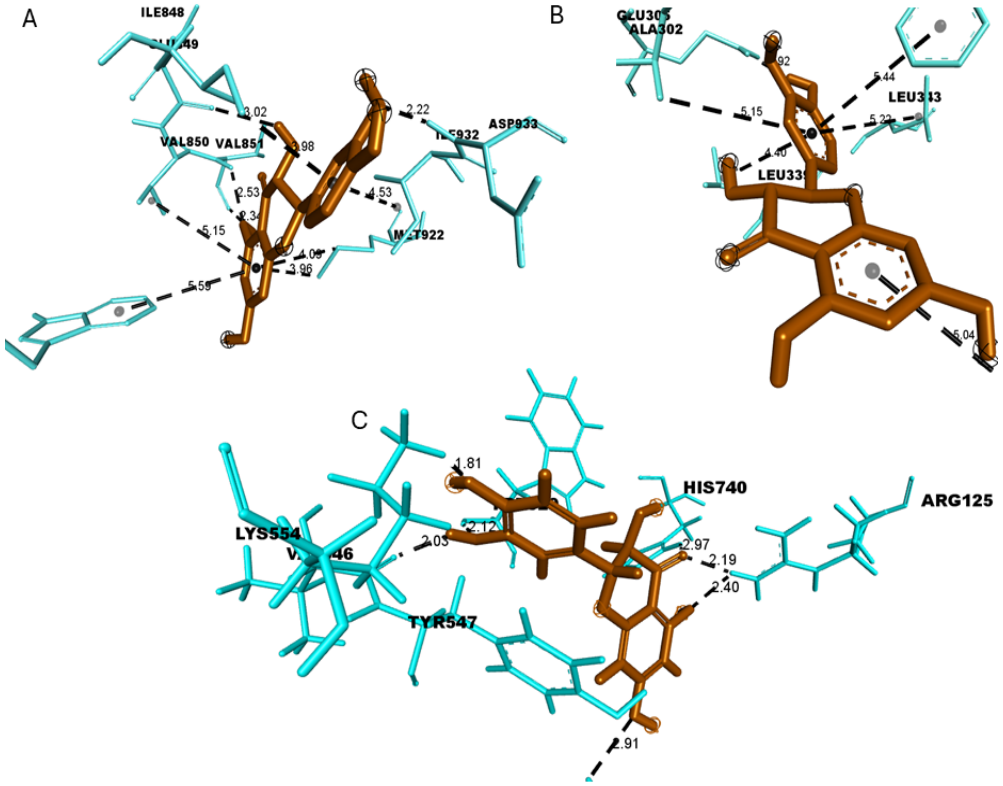

Figure 14: Interaction distances between taxifolin-8XEL complex (A), taxifolin-3OLL complex (B), and taxifolin-5T4B complex (C) with respective amino acid residues.

From the docking analysis, complexes with binding scores below –40 kcal/mol were selected for detailed examination. Figures 14A–B reveal that these two selected complexes had distant ligand–residue contacts (1.81–5.58 Å) in comparison to the 5T4B–Taxifolin complex. In the 5T4B–Taxifolin complex, hydroxyl groups at positions 3 and 4 of Taxifolin formed short, directional hydrogen bonds with the guanidinium side chain of Arg125 (2.40 and 2.19 Å). Although these are hydrogen bonds rather than typical salt bridges, their pattern mimics salt bridge stabilization by combining strong hydrogen bonds with electrostatic support from Arg125 (see Figure 14). Additional contacts within 1.81–3.0 Å were observed, indicating a more constrained binding geometry than in other complexes. This distinct interaction, which was absent in other complexes, likely explains the more favourable docking score. Therefore, the 5T4B–Taxifolin complex was selected for further validation using single-point MM-PBSA calculations.

A single-point MMPBSA analysis was conducted on the top-docked complex, revealing a complex energy of -1718.72 Kcal/mol (Figure 15). The system's favourable energy suggests that this protein could serve as a promising molecular target for further optimization and validation. However, docking results alone are insufficient, so additional molecular dynamics simulations are necessary.

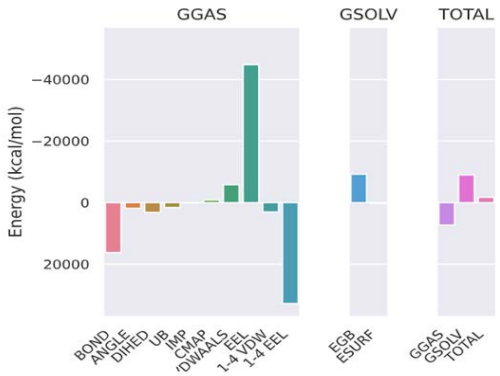

Figure 15: Single point MMPBSA of 5T4B-Taxifolin docked complex energy performed with gmx MMPBSA.

Molecular dynamics simulation

Molecular dynamics (MD) simulation is a suitable technique for examining the kinetic stability of ligands in the active site of the selected target and the contribution of key amino acids to the interaction between the ligand & protein. The Taxifolin molecule shows a higher docking score with the 5T4B receptor than with other Alzheimer's target receptors, so it was subjected to a 100ns Molecular Dynamics simulation to better understand

its stability & interaction dynamics. Molecular dynamics simulations were run in triplicate, 1 from the original system setup & 2 others started with different random initial velocities to ensure statistical robustness.

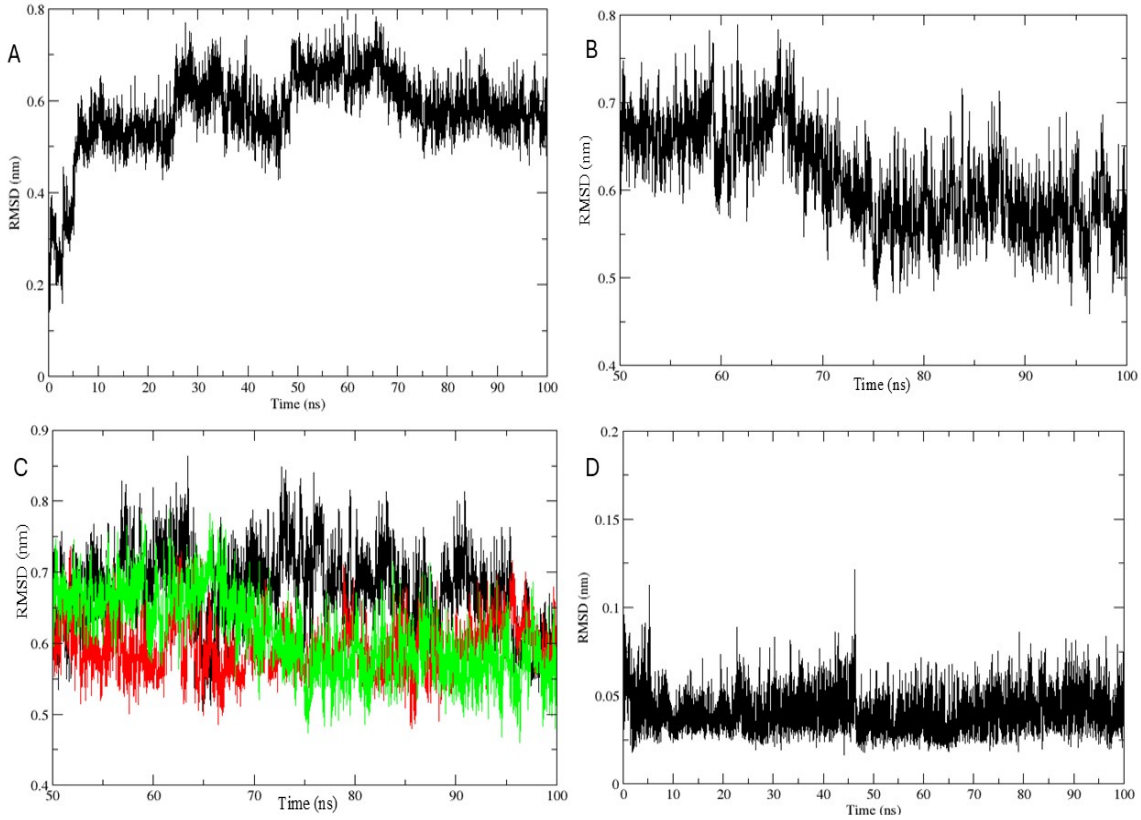

Figure 16: RMSD of protein ligand complex (A), Stable RMSD from 50ns to 100ns (B), triplicate RMSD from independent three runs with different initial velocities were shown (C), Ligand RMSD (D).

Figure 16 A shows the RMSD of the 53TB -Taxifolin complex. Between approximately 10 and 40 ns, the RMSD fluctuates between 0.4 and 0.5 nm, indicating a relatively stable state. Between 40–100 ns, RMSD data points show slight shifts to about 0.5–0.65 nm, but no larger drifts are observed. Therefore, the complex equilibrates by around 10 ns and remains stable through 100 ns, with only moderate fluctuations. Figure 16B displays the RMSD in the 50–100 ns window, ranging from 0.55 to 0.65 nm, indicating increased stability in this region.

Since the system is equilibrated and stable, trajectories from 50 to 100 ns were used for further analysis, including free energy binding, RMSF, and gyration. Figure 16 C presents triplicate RMSDs from 3 independent runs with different initial velocities. All three runs (black, red, green) fluctuate within a similar RMSD range of about 0.55–0.75 nm. The reproducibility across these independent simulations validates the MD approach. Figure 11 D illustrates the ligand RMSD, which is very low, approximately 0.05–0.1 nm, and remains stable throughout the entire 100 ns simulation. The ligand maintains its binding pose with minimal movement, strongly indicating stable binding.

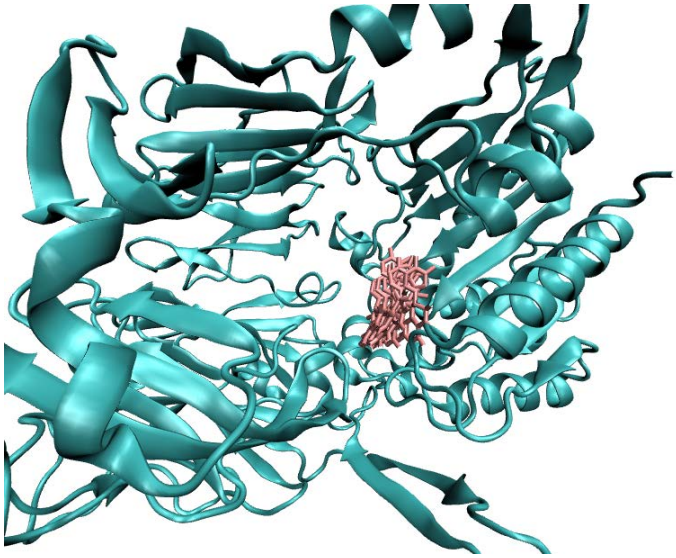

Figure 17: The conformational changes of the ligand at every 10ns. Captured using VMD.

Every 10 ns conformation of Taxifolin obtained from the MD trajectory (Figure 17) confirms that the ligand stayed within the same binding pocket of the protein, which is consistent with the stable ligand RMSD profile observed during the simulation (Figure 18D).

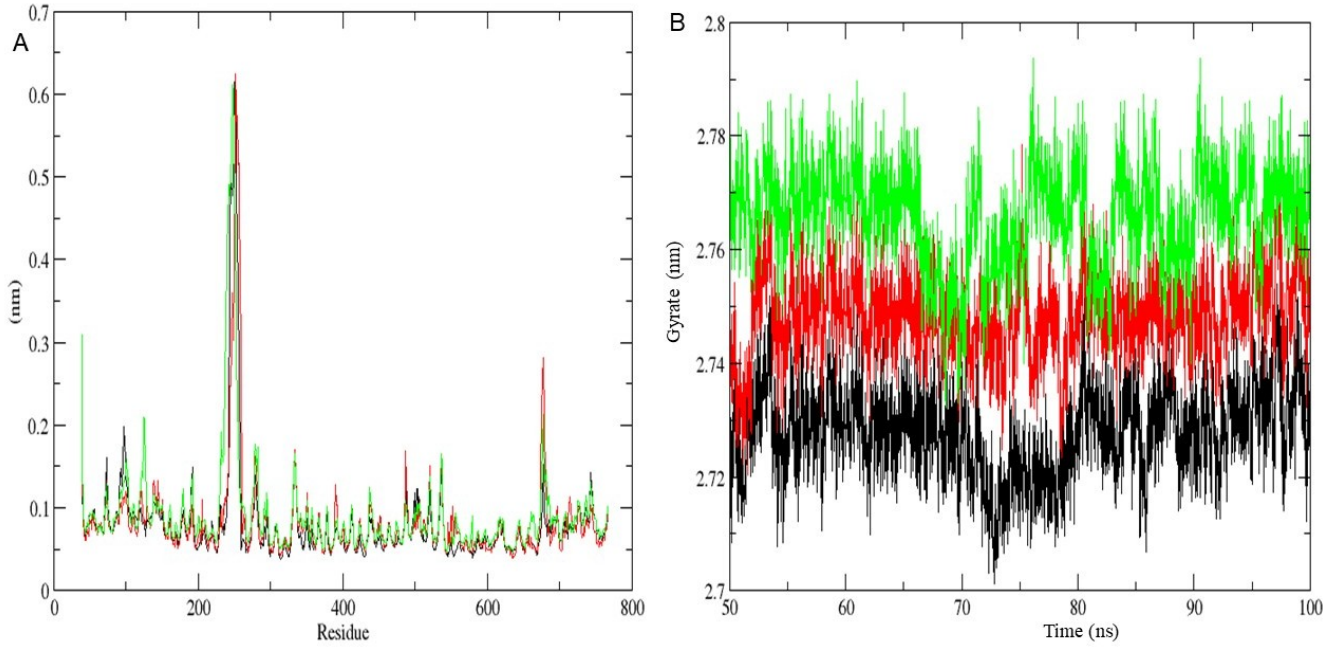

Figure 18: Root mean square fluctuation of amino acid residues upon ligand binding (A), Stable RMSD from 50ns to 100ns. B radius of gyration of the last stable 50ns.

The Root Mean Square Fluctuation per residue (RMSF) was determined for the 5T4B-taxifolin complex. The y-axis shows fluctuations (in nm) and the x-axis shows residue number. Most residues exhibit low fluctuations, approximately 0.1 nm, indicating overall structural rigidity. A sharp peak around residue 200 suggests a flexible loop region. The low RMSF across most residues suggests that the ligand binding stabilizes the protein backbone except for certain flexible regions (Figure 18A). Figure 20B shows the radius of gyration (Rg values), which fluctuate between 2.72 & 2.78 nm, with three trajectories (black, red & green) displayed. Each replicate shows a consistent trend with minor deviations, suggesting reproducibility. The protein maintains its compactness during the last 50 ns.

Figure 19 shows the number of hydrogen bonds formed between the protein and ligand. The protein–ligand complex creates dynamic hydrogen bonds ranging from 0 to 7 throughout the 100 ns trajectory. On average, 3–4 hydrogen bonds are maintained, with the strongest binding phase occurring between 50–70 ns.

Figure 20 A–C shows the number of H-bonds over time for residues 553, 666, and 670, while Figure 20 D–F shows the corresponding donor–acceptor distances over time. The hydrogen bond occupancy percentage was calculated using VMD and listed in Table 7. Hydrogen-bond analysis of key residues (GLN553, TYR666, TYR670) with the ligand revealed dynamic yet transient interactions throughout the 100-ns trajectory. GLN553 formed the most stable hydrogen bond (16.77% occupancy), with an average donor–acceptor distance of approximately 0.15 nm. TYR670 showed moderate hydrogen-bond occupancy of 6.09%, with an average distance of about 0.19–0.20 nm.

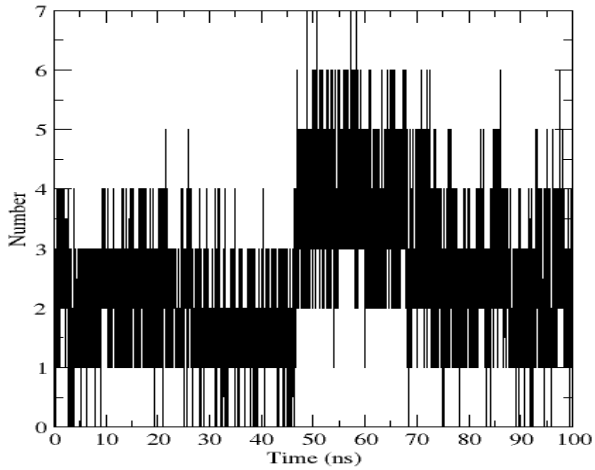

Figure 19: The number of hydrogen bonds formed throughout the simulation.

TYR666 contributed minimally at 3.39%, with a distance of roughly 0.165 nm. None of the residues maintained an occupancy greater than 20%, indicating that these hydrogen bonds are transient rather than persistent. The ligand's binding might be driven more by hydrophobic or van der Waals interactions than polar contacts. Therefore, the solvent-accessible surface area was calculated to assess the nonpolar nature of the binding.

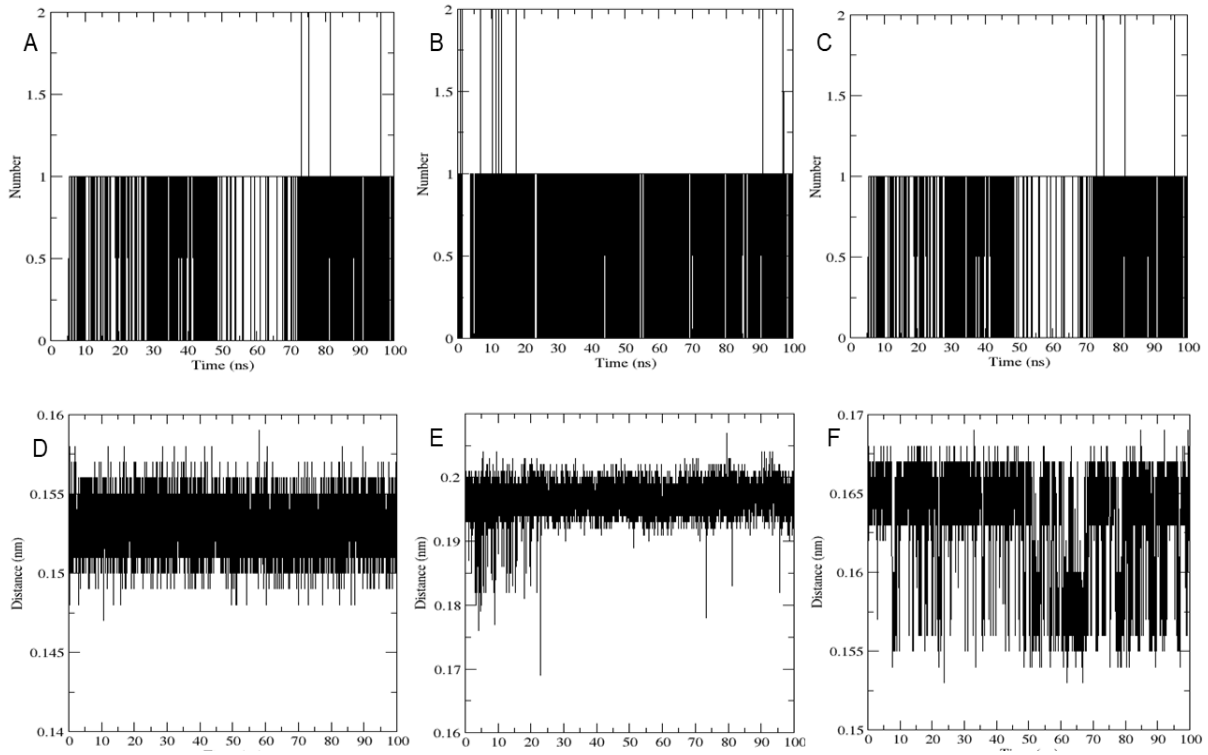

Figure 20: The number of hydrogen bonds formed between the amino acid residues 553, 666, and 670. A, B, and C show the distance between the amino acid residues (553, 666, and 670) and the taxifolin ligand.

Table 7: The hydrogen bond occupancy percentage of each donor and acceptor residue for the last 50ns.

Donor	Acceptor	Occupancy
HIS740-Side	LIG767-Side	0.60%
TYR547-Side	LIG767-Side	0.23%
ARG125-Side	LIG767-Side	0.03%
GLN553-Main	LIG767-Side	16.77%
SER630-Side	LIG767-Side	1.10%
LYS554-Side	LIG767-Side	0.02%
TYR666-Side	LIG767-Side	3.39%
TYR670-Side	LIG767-Side	6.09%
ARG669-Side	LIG767-Side	0.01%
SER209-Side	LIG767-Side	0.07%
TYR585-Side	LIG767-Side	0.43%
ARG358-Side	LIG767-Side	2.20%

The Solvent Accessible Surface Area (SASA) plot (Figure 21A) shows fluctuations between 4.4 and 5.4 nm² over 100 ns. The ligand maintains a consistent level of solvent exposure while remaining bound to the protein. The distance between hydrophobic residues and the ligand (Figure 21B) fluctuates approximately around 1.5–1.6 nm, which is very little across the 100 ns simulation. This consistent close interaction indicates that hydrophobic residues are stably engaging with the ligand.

From the SASA plot, hydrophobic contacts might play an essential role in stabilizing the ligand–protein complex, rather than polar hydrogen-bond contacts.

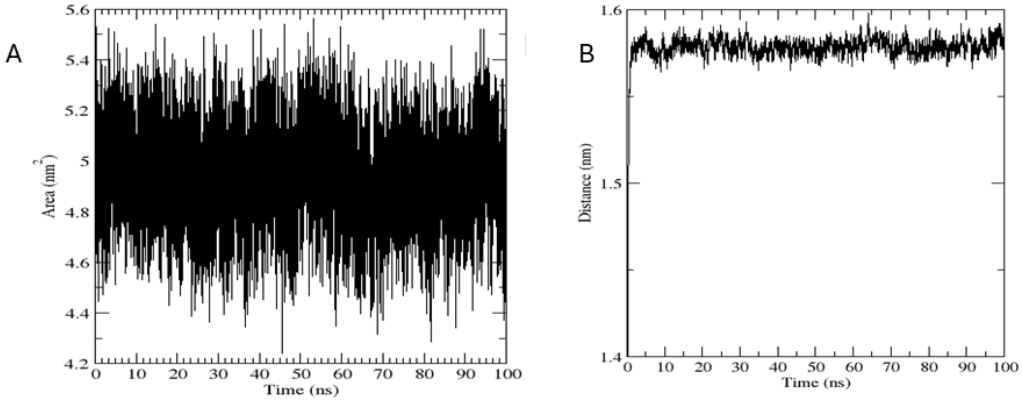

Figure 21: The SASA of the ligand 4.2 -5.6 nm² shows partially solvent-exposed continuous timescale fluctuations with no major shifts (B). C shows the distances between the hydrophobic amino residues and the ligand.

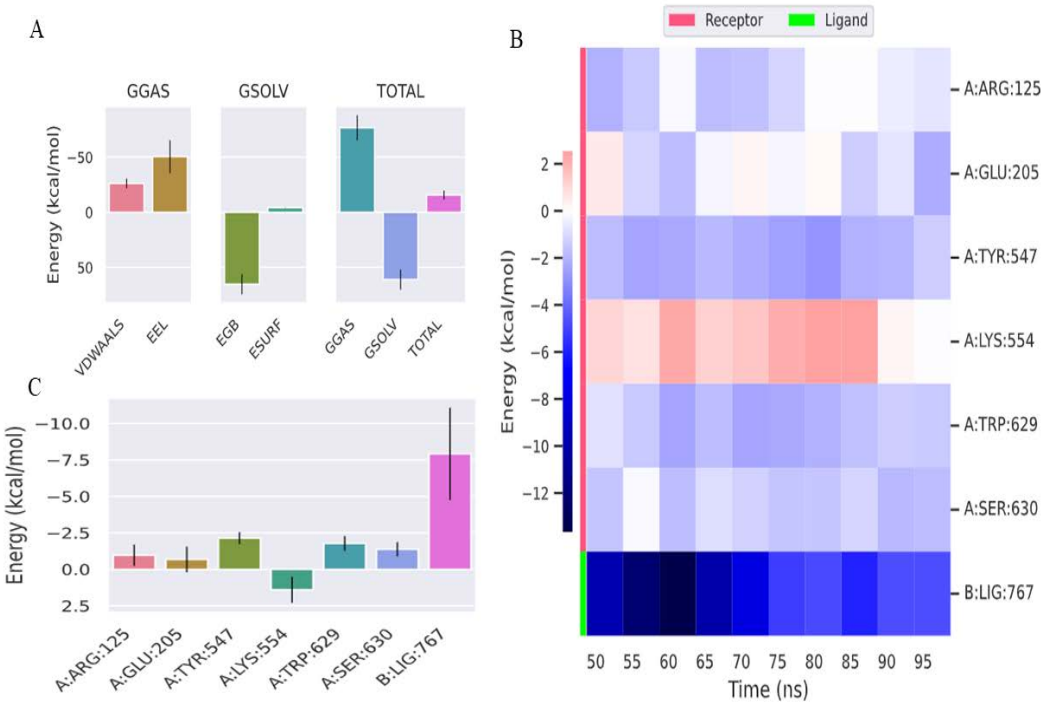

Figure 22: MMPBSA results of protein ligand simulation. Protein ligand binding free energy (A). Heat map of decomposition energies of each residue with timelines from 50ns (B). Per residue decomposition energy contributed over the last 50 ns (C).

Table 8: Protein ligand complex energy from MMPBSA analysis by gmx ana for the last 50ns stable simulation period. The average MMPBSA from three independent runs was found to be -18.5 Kcal/mol.

Delta (Energy Component)	MD run 1 Average Kcal/mol	SD	MD run 2 Average Kcal/mol	SD	MD run 3 Average Kcal/mol	SD
ΔBOND	0	±1.11	0	±1.11	0	±1.78
ΔANGLE	0	±1.44	0	±1.44	0	±2.93
ΔDIHED	0	±2.09	0	±2.09	0	±2.15
ΔUB	0	0	0	0	0	0
ΔIMP	0	±0.12	0	±0.12	0	±0.07
ΔCMAP	0	0	0	0	0	0
ΔVDWAALS	-26.18	±0.05	-22.04	±0.05	-21.81	±0.06
ΔEEL	-50.46	±2.05	-60.37	±2.05	-60.14	±2.15
Δ1-4 VDW	0	0	0	±1.73	0	±1.57
Δ1-4 EEL	0	0	0	±3.36	0	±1.08
ΔEGB	65.13	±1.56	72.03	±1.56	72.03	±0.3
ΔESURF	-4.2	±0.03	-5.2	±0.03	-5.20	±0.04
ΔGGAS	-76.64	±2.05	-93.02	±2.05	-93.02	±1.92
ΔGSOLV	60.94	±1.56	65.62	±1.56	65.62	±0.3
ΔTOTAL	-15.71	±2.58	-21.16	±2.58	-18.88	±1.82

MMPBSA analysis

Figure 22A shows the protein ligand binding free energy VDWAALS (van der Waals), ESURF (nonpolar solvation), is negative, and particularly EEL (electrostatics) shows strongly negative and drives ligand binding and stability. The net binding energy over the last 50 ns of the stable simulation was found to be -18.8 Kcal/mol using MMPBSA gmx ana. The ligand–protein complex is primarily stabilized by electrostatic & van der Waals interactions, which are partially offset by the desolvation penalty. A heat map was created for the provided frames, displaying the interaction energy contributions of each amino acid residue (Figure 22B). The color scale (red/blue) depicts the interaction energy contribution (kcal/mol) between the residue and the ligand. Blue (negative values) shows ligand-stabilizing

interactions that favor binding, while red (positive values) indicates destabilizing interactions. The heatmap displays the contributions of residue fluctuation over time in nanoseconds. LIG:767 (ligand) remains dark blue, indicating strong and stable binding. TRP629 and SER630 also consistently show blue, suggesting stabilization. LYS554 displays red patches, which, at times, unfavorably contribute and may cause electrostatic repulsion. Other residues (ARG125, GLU205, TYR547) contribute weak/moderate interactions. Figure 22 C confirms the trends in the heatmap. TRP629 and SER630 show favorable (negative) contributions, while LYS554 indicates an unfavorable contribution. The ligand (B: LIG:767) has a significant negative energy, making it a strong stabilizer. Others like ARG125, GLU205, TYR547 contribute minimally.

LIMITATIONS AND FUTURE ASPECTS

A Limitation of this study is the relatively small number of overlapping targets used for enrichmnet analysis, which may reduce statistical power after multiple testing corrections. Future studies using large datasets or experimental validation are warranted. The TPSA of taxifolin is 127, so it couldn't cross the blood-brain barrier, as predicted by this in silico analysis. This will be helpful for the researcher in designing a suitable drug delivery system for Taxifolin. If the drug is able to penetrate the BBB, then it will be a suitable candidate to treat Alzheimer's disease. Most natural bioactive molecules, due to their poor solubility or permeability and high molecular weight, are unable to cross the BBB to produce their biological activities. There are many drug delivery technologies, such as nanoparticles, liposomes, micelles, and dendrimers, that enhance the penetration of active molecules [14]. It enhances drug solubility, stability, and protection from enzymatic degradation at the site of action. Its small size facilitates transport across the BBB via transcytosis and endocytosis. As Liposomes resemble biological membranes, they can interact with the endothelial cells of the BBB and release the drug in a sustained manner. Dendrimers offer high surface functionality, allowing ligand attachment for receptor-mediated BBB targeting. Polymeric nanoparticles provide controlled release and prolonged circulation time, increasing brain exposure [15].

Micelles efficiently encapsulate hydrophobic natural compounds and improve passive diffusion across the BBB. Surface modification with PEG or targeting ligands further enhances BBB penetration. Hence, these strategies offer promising solutions for the treatment of neurological disorders using plant-derived therapeutics such as Taxifolin.

CONCLUSION

Network pharmacology and docking often neglect receptor flexibility and solvent effects, potentially reducing predictive accuracy. Molecular dynamics simulations are limited in that they can only sample a fraction of the conformational space accessible to the complex, and some rare alternative binding modes that occur on longer time scales may not be fully captured. Hence, in our future studies, these computational findings will be supported by experimental validation.

FINANCIAL ASSISTANCE

NIL

CONFLICT OF INTEREST

The authors declare no conflict of interest.

AUTHOR CONTRIBUTION

Ashif Anjukandan contributed to the study's conceptualization, methodology, resource collection, and preparation of the original draft of the manuscript. K. Rajaganapathy supervised the overall work and was responsible for reviewing, editing, and correcting the manuscript.

REFERENCE

[1] Better M, Mapping A. Alzheimer's disease facts and figures. *Alzheimers Dement.*, **19**, 1598–1695 (2023) https://doi.org/10.1002/alz.13809

[2] Zhang XX, Tian Y, Wang ZT, et al. The epidemiology of Alzheimer's disease modifiable risk factors and prevention. *J. Prev. Alzheimers Dis.*, **8**, 313–321 (2021) https://doi.org/10.14283/jpad.2021.15

[3] Qiu C, Kivipelto M, von Strauss E. Epidemiology of Alzheimer's disease: occurrence, determinants, and strategies toward intervention. *Dialogues Clin. Neurosci.*, **11**, 111–128 (2009) https://doi.org/10.31887/DCNS.2009.11.2/cqiu

[4] Blennow K, de Leon MJ, Zetterberg H. Alzheimer's disease. *Lancet*, **368**, 387–403 (2006) https://doi.org/10.1016/S0140-6736(06)69113-7

[5] Qiu C, Kivipelto M, Aguero-Torres H, Winblad B, Fratiglioni L. Risk and protective effects of the APOE gene towards Alzheimer's disease in the Kungsholmen project: variation by age and sex. *J. Neurol. Neurosurg. Psychiatry*, **75**, 828–833 (2004) https://doi.org/10.1136/jnnp.2003.021493

[6] Zhang C, Wang Y, Wang D, Zhang J, Zhang F. NSAID exposure and risk of Alzheimer's disease: an updated meta-analysis from

cohort studies. *Front. Aging Neurosci.*, **10**, 83 (2018) https://doi.org/10.3389/fnagi.2018.00083

[7] Singh B, Day CM, Abdella S, Garg S. Alzheimer's disease current therapies, novel drug delivery systems and future directions for better disease management. *J. Control. Release*, **367**, 402–424 (2024) https://doi.org/10.1016/j.jconrel.2024.01.047

[8] Debraj Dey, Roy Mukherjee D, Shoeb A, Biswas P, Santra S. A systematic review of Alzheimer's disease: exploring genetic and environmental risk factors, biomarkers, and future pharmacotherapy for cognitive decline and neurodegeneration. *J. Appl. Pharm. Res.*, **13**, 17–35 (2025) https://doi.org/10.69857/joapr.v13i3.929

[9] Liu Y, Shi X, Tian Y, Zhai S, Liu Y, Xiong Z, Chu S. An insight into novel therapeutic potentials of taxifolin. *Front. Pharmacol.*, **14**, 1173855 (2023) https://doi.org/10.3389/fphar.2023.1173855

[10] Khan S, Bano N, Ahamad S, John U, Dar NJ, Bhat SA. Excitotoxicity, oxytosis/ferroptosis, and neurodegeneration: emerging insights into mitochondrial mechanisms. *Aging Dis.*, **16**, 2504–2543 (2024) https://doi.org/10.14336/AD.2024.0125

[11] Chang Y, Hawkins BA, Du JJ, Groundwater PW, Hibbs DE, Lai F. A guide to in silico drug design. *Pharmaceutics*, **15**, 49 (2023) https://doi.org/10.3390/pharmaceutics15010049

[12] Ekins S, Mestres J, Testa B. In silico pharmacology for drug discovery: methods for virtual ligand screening and profiling. *Br. J. Pharmacol.*, **152**, 9–20 (2007) https://doi.org/10.1038/sj.bjp.0707305

[13] Wu F, Zhou Y, Li L, Shen X, Chen G, Wang X, Liang X, Tan M, Huang Z. Computational approaches in preclinical studies on drug discovery and development. *Front. Chem.*, **8**, 726 (2020) https://doi.org/10.3389/fchem.2020.00726

[14] Balagurusamy B, Ganesan V, Gopi V, Ilayaperumal P. Liposomal and nanomaterial-based strategies for targeted Alzheimer's disease therapy. *ACS Omega*, **10**, 60004–60019 (2025) https://doi.org/10.1021/acsomega.5c05391

[15] Asil SM, Ahlawat J, Barroso GG, Narayan M. Nanomaterial-based drug delivery systems for the treatment of neurodegenerative diseases. *Biomater. Sci.*, **8**, 4109–4128 (2020) https://doi.org/10.1039/D0BM00809E